Physica Medica 138 (2025) 105182

Contents lists available at ScienceDirect

Physica Medica

journal homepage: www.elsevier.com/locate/ejmp

Original paper

Evaluation of MR-driven versus MR-free PET/CT spatial normalization approaches for quantification of regional uptake in Dementia

Francesco Grassi [a,1], Mario Verdicchio [a,b,*,1], Carlo Cavaliere [a], Vincenzo Alfano [a], Marco Cerrone [a], Angelica Di Cecca [a,c], Elena Salvatore [a,d], Emanuele Nicolai [a], Marco Salvatore [a], Sabina Pappatà [a], Marco Aiello [a]

[a] IRCCS SYNLAB SDN, Via Gianturco 113, Naples, 80143, Italy
[b] Università degli Studi di Napoli Federico II - DIETI, Via Claudio 21, Naples, 80125, Italy
[c] Università degli Studi di Napoli Federico II - DNRSO, Via Sergio Pasini 5, Naples, 80131, Italy
[d] Università degli Studi di Napoli Federico II - DISBA, Via Sergio Pasini 5, Naples, 80131, Italy

ARTICLE INFO

Keywords:
PET spatial normalization
PET-FDG
Amyloid PET

ABSTRACT

Background: Spatial normalization is a critical preprocessing step in PET imaging. While MR-driven normalization represents the gold standard, MR-free approaches offer an alternative that may enhance accessibility.
Purpose: This study aims to evaluate the performance of MR-free normalization compared to MR-driven normalization across three PET modalities (18F-FDG, early-phase amyloid, and late amyloid PET), examinating regional agreement.
Methods: 56 patients with dementia performing MR and the three PET modalities were retrospectively enrolled in the study. Three different spatial normalization methods were performed: MR-driven and two MR-free (^{15}O-H_2O template and site-specific PET template). The agreement among different methods was pair-wise compared using intraclass correlation coefficients (ICCs).
Results: MR-free normalization showed strong agreement with MR-driven methods for FDG and early amyloid PET, with ICCs > 0.99 in cortical regions. The spatial normalization with early-phase amyloid site-specific template had a median ICC of 0.927, confirming its agreement with MR-driven approach. The performance was slightly lower with late amyloid-derived templates (ICC = 0.822) compared to the ^{15}O-H_2O template. The worst reproducibility was observed in cerebellar and thalamic sub-regions, though aggregating sub-ROIs in parent regions brought to strong ICCs (> 0.920).
Conclusion: MR-free normalization is a viable alternative to MR-driven approaches, particularly for FDG and early amyloid PET. In addition, the results confirm the similarity of early amyloid and FDG tracers distributions.

1. Introduction

Dementia is a syndrome characterized by a significant cognitive decline, commonly linked to neurodegenerative disorders, with Alzheimer's disease (AD) being the most prevalent form [1]. Despite their heterogeneity, all dementias share key pathological mechanisms, such as abnormal protein accumulations and metabolic alterations that impair neuronal function [2]. Positron emission tomography (PET) is essential for diagnosing and studying dementia, allowing in vivo observation of neurodegenerative processes [3]. Among these, 18F-fluorodeoxyglucose PET (18F-FDG PET) is widely used to detect reduced glucose metabolism, a marker of neurodegeneration [4]. Additionally, amyloid PET imaging enables in vivo detection of beta-amyloid ($A\beta$) plaques, a hallmark of AD [5]. The use of 18F-labeled amyloid tracers, such as 18F-florbetapir, 18F-florbetaben, and 18F-flutemetamol, provides a valuable tool for visualizing and quantifying amyloid burden in the brain [6].

Dual-phase amyloid PET has emerged as a new acquisition modality, capturing early-phase images after tracer injection reflecting cerebral perfusion, alongside standard late-phase scans for amyloid plaque

* Corresponding author at: IRCCS SYNLAB SDN, Via Gianturco 113, Naples, 80143, Italy.
E-mail addresses: mario.verdicchio@synlab.it, mario.verdicchio@unina.it (M. Verdicchio).
[1] These authors contributed equally to this work.

https://doi.org/10.1016/j.ejmp.2025.105182
Received 19 March 2025; Received in revised form 1 September 2025; Accepted 13 September 2025
Available online 3 October 2025

detection. This approach may assess both amyloidosis and neurodegeneration in a single scan. Early-phase amyloid PET images have shown strong similarities with FDG PET images, demonstrating their potential as markers of neuronal damage [7].

A crucial aspect of quantitative PET image analysis is spatial normalization, that transforms individual PET images into a standard anatomical space. It is important for accurate regional or voxel-based quantification, enabling comparisons between subjects and the application of Region of Interest (ROI) atlases or voxel-based analysis.

Over the last 20 years, several approaches have been proposed for regional quantification of PET in brain images. They can be broadly classified into MR-driven approaches [8–11] and MR-free [12–14]. Among these, the theoretical superiority of MR-driven approaches is intuitively understandable, due to the high spatial resolution and soft tissue contrast of MR compared to PET. MR-based spatial normalization typically relies on an individual MR image and an MR template for automatic ROI and voxel-based analysis. However, MR imaging may be not always available. Therefore, assessing the feasibility of standalone PET/CT approaches becomes essential, particularly for individuals with neurological diseases. Several studies have explored PET template-based spatial normalization generated by averaging spatially aligned images [15]. These templates can be tracer-specific, derived from images of the same tracer, or population-specific, designed to account for variations in brain morphology in a specific patient cohorts [15].

A commonly used reference perfusion based template is the standard oxygen-15-labeled water ($^{15}O - H_2O$)template provided by SPM [16]. Depending on the tracer, such as [18F]-FDG, regional tracer uptake may not match the blood flow-based signal pattern of the $^{15}O-H_2O$ template. This misalignment can interfere with accurate normalization, as the individual's FDG brain features may not align with the template. To address this, Della Rosa et al. [17] proposed a site-specific FDG template tailored for dementia populations, accounting for the unique brain activity patterns observed in these patients. Spatial normalization of PET amyloid images using the PET-template approach is more critical as these images have limited anatomical information and the regional amyloid PET radioactive concentration is different between amyloid negative and positive subjects. The use of PET template created from early perfusion-related images has been proposed as an alternative approach and tested in few AD patients and controls [18].

The present study aims to systematically compare for the first time MR-driven versus MR-free spatial normalization techniques on regional uptake values in a cohort of dementia patients, using three different PET imaging modalities: 18F-flutemetamol amyloid PET, early-phase amyloid PET (eFMM), and 18F-FDG PET. To achieve this, for each PET modality, three different templates were generated: one driven by MR and two MR-free. Pairwise comparisons between the MR-driven template and the two MR-free templates were conducted to evaluate the feasibility and reliability of PET quantification in the absence of structural MRI data.

2. Material and methods

2.1. Study sample and imaging acquisition protocol

A group of 56 dementia patients (25 females, average age 65.19 ±7.93; 31 males, average age 67 ±7.70) participated in this study, approved by the local ethics committee. All participants gave written informed consent. Each patient underwent MRI examinations along with FDG and amyloid PET/CT scans. Analysis of amyloid uptake revealed that 30 patients tested positive (Amyloid +), while 26 tested negative (Amyloid -). The acquisition parameters relating to the images used in this work will be specified in detail below. Amyloid-PET acquisition was performed 60–480 s (early amyloid) and 90-110 min (late amyloid) after intravenous injection of [18F]flutemetamol (dose range: 180–190 MBq). FDG-PET acquisition was performed 40-50 min after intravenous injection of [18F]-FDG (dose range: 200–250 MBq). All PET images were acquired in a GE Discovery PET/CT 710 scanner in 3D scanning mode, including 47 slices of 3.3-mm thickness. Images reconstructed using 3D iterative ordered-subset expectation maximization (OSEM) using attenuation-weighted iterative reconstruction (7 iterations, 36 subsets). 3D T1-weighted were acquired on a 3T scanner (Philips Achieva dStream or Siemens Biograph mMR) following a harmonized protocol (1 mm isotropic resolution; TE=3.73 ms; TR=8.18 ms; FA=8°; FOV=240 × 240x180 mm).

To ensure clarity, amyloid PET data will henceforth be referred to as "Amyloid", early-phase amyloid PET data as "Early Amyloid", and FDG PET data as "FDG".

2.2. Template generation

A robust template creation process is essential to perform spatial normalization in PET imaging [15]. Technically, spatial normalization is a registration procedure between an individual image and a template. This process involves constructing a representative anatomical template that reflects the typical brain structure and functional regions in a specific population.

In this study, following the approach proposed by Gispert et al. [19], three spatial normalization were performed for each PET modality. In particular, the following methods were used:

1. MR-driven normalization
2. Site-specific PET template
3. Standard PET template

2.2.1. MR-driven normalization

The normalization process, driven by the MRI, was used to transform the PET images from their native space to the common MNI (Montreal Neurological Institute) [20] space. The steps of the registration procedure are outlined in Part A of Fig. 1. First, T1-weighted MRI (T1-w) was registered on the MNI template with a multistep process that involved rigid, affine and nonlinear transformations, performed by ANTs (Advanced Normalization Tools) [21]. The rigid-body transformation was applied with a gradient step size of 0.05 to align the two images using the Mattes mutual information (MI) metric [22]. An affine transformation was then performed with a gradient step size of 0.08, using the same Mattes mutual information metric as in the rigid stage. Finally, a non-linear transformation using the Symmetric Normalization (SyN) algorithm [23] was applied with a step size of 0.1 using the cross-correlation (CC) [24] as a metric for the optimization.

Subsequently, the CT image was aligned with the T1-w MRI using a rigid body (linear) transformation with Mattes mutual information (MI) as a metric. By applying the transformation parameters resulting from CT-to-T1 registration, the PET image – already co-registered with CT – was subsequently registered on T1 w. Then using the parameters obtained from T1-w to MNI template normalization, PET images were normalized to the MNI template.

2.2.2. Site-specific PET template

Using the PET images normalized to MNI space from the MR-driven procedure described before, a site-specific template can be generated by averaging these normalized PET images from all of the subjects involved in the study. This template can be used to normalize PET images of additional subjects, serving as a reference for future analyses.

2.2.3. Standard PET template

The last approach is tailored to specific radiotracers, allowing differentiation between early amyloid, FDG, and amyloid imaging. For the first two, the standard reference is the oxygen-15-labeled water ($^{15}O - H_2O$)template provided by SPM [16]. This template was created by averaging 12 PET scans of subjects in normal resting conditions with their eyes closed. In this study, the normalization process was performed using a non-linear transformation with ANTs, similar to the

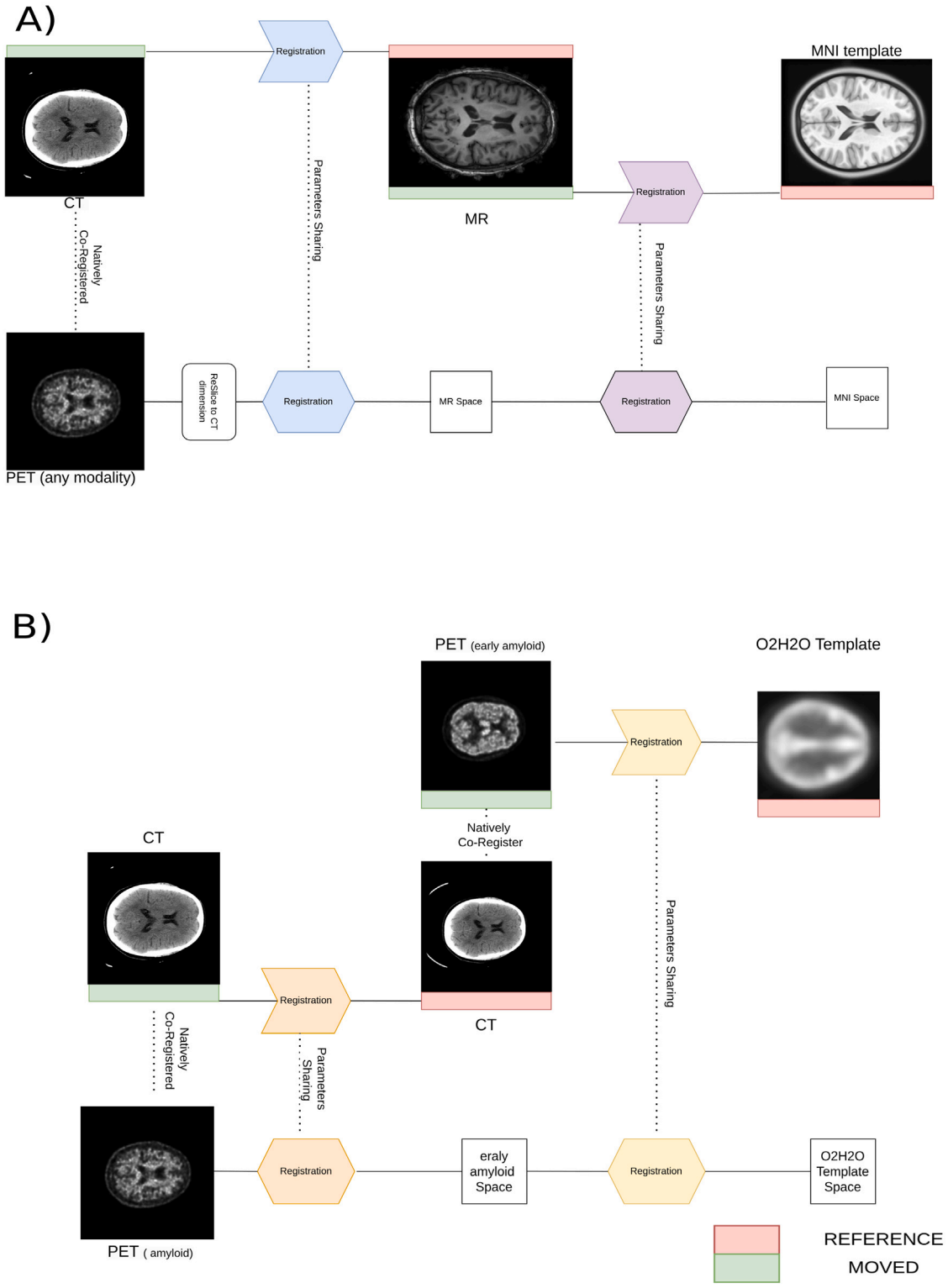

Fig. 1. Workflow Diagrams. (A) MR-Driven Template: Workflow for T1-w MRI registration to MNI Template, followed by PET normalization taking advantage of the natively co-registered CT. (B) Standard Template: For amyloid PET normalization, a co-registration between early and late phases is performed using CT as an intermediary.

MR-driven normalization described earlier, but in this case, the mutual information (MI) metric was used for all three transformation steps. A slightly different approach must be considered for amyloid imaging, as the nature of the tracer and the imaging target differ from perfusion tracers. In amyloid imaging, the PET tracer binds to amyloid plaques in the brain, resulting in a distinct spatial distribution compared to tracers that measure blood flow or metabolism. In this context, the method proposed by Ing-Tsung Hsiao et al. [18] involved registering the early phase of amyloid imaging with the amyloid phase.

In this paper, an additional step was introduced, involving a prior co-registration between the early and standard phases of amyloid imaging using the CT image as an intermediary. This process is summarized

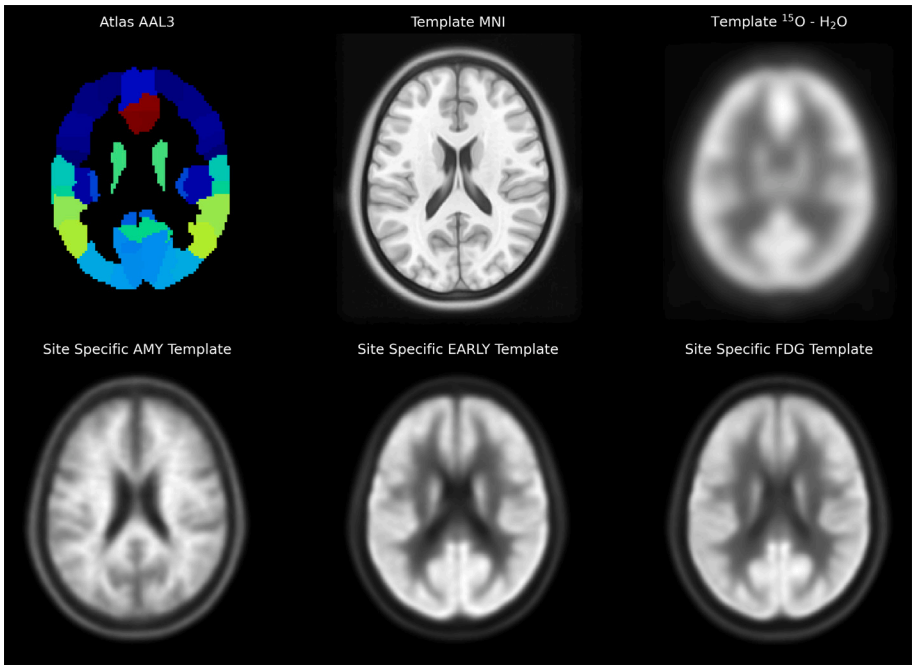

Fig. 2. Axial views of six brain templates and atlases used in the study. First row shows AAL3 Atlas used for brain region parcellation, the standard MNI and $^{15}O - H_2O$ template. Second row shows the site-specific templates created in the study for each of the three modalities considered.

in Part B of Fig. 1. In Fig. 2 an axial view of the Site-specific templates created is provided.

Following the same schema, an additional normalization strategy was performed for FDG images using the template proposed by Della Rosa et al. [17]. This template was created as an alternative to the $^{15}O - H_2O$ template for patients with dementia, making it comparable to a site-specific template. To create it, a total of 120 FDG PET images were used, comprising 60 from healthy subjects and 60 from patients with dementia. The $^{15}O - H_2O$ template was considered in our main analysis as its use provided a consistent reference point, facilitating coherence and reliability in comparative evaluations.

3. Statistical analysis

To assess the differences among various normalization strategies, regional uptake values were compared across all regions of interest (ROIs) defined in Automated Anatomical Labeling Atlas (AAL3) [25]. This analysis ensures a consistent interpretation of PET imaging results.

The evaluation process was summarized in algorithm 1.

The leave-one-out procedure was adopted to validate the site-specific template. In this way, the arrival of a new subject was simulated. This approach involves excluding one subject at a time from the dataset and using the remaining data to construct the template. The excluded subject is then used for testing to evaluate the effectiveness of the template, simulating the introduction of a new subject.

The consistency of the regional uptake values across the three template strategies were evaluated using the two-way mixed-effects Intraclass Correlation Coefficient (ICC) [26], ICC(3,1) [27] defined this way:

$$ICC(3,1) = \frac{MS_r - MS_e}{MS_r + (k-1)MS_e} \quad (1)$$

Where:

- MS_r: Mean Square for rows (i.e, between scanner measurements)
- MS_e: Mean Square for error
- k: The number of measurements.

Algorithm 1 Evaluation Procedure

Phase 1 – Normalization

procedure NORMALIZATION PROCEDURE
  for each subject $j \in [1, N]$ **do**
    MR-driven Normalization
    Standard Normalization
    procedure LEOVE ONE OUT TEMPLATE CREATION
      $T_j = \frac{1}{N-1} \sum_{\substack{i=1 \\ j \neq i}}^{N} PETmni_i$
      Normalize jth subject using T_j
    end procedure
  end for
end procedure

Phase 2 – Uptake Evaluation

for each normalization modality $n \in [MR-driven, Site-Specific, Tracker-Specific]$ **do**
  for each subject $j \in [1, N]$ **do**
    Calculate regional uptake
  end for
  Aggregate uptake results
end for

This model was chosen because it measures the reliability of measurements across different raters or conditions, in this case, the three template strategies. ICC values were calculated for each ROI and each modality (Amyloid, Early amyloid, FDG) to evaluate the level of agreement between the different template strategies. Particular attention was given to the consistency between the templates generated with and without MRI guidance. A higher ICC ($ICC > 0.75$) value indicates stronger agreement, suggesting that different templates produce consistent regional uptake values.

To account for the trend in pair-wise comparisons, the median of the Intraclass Correlation Coefficient (ICC) was calculated. The median

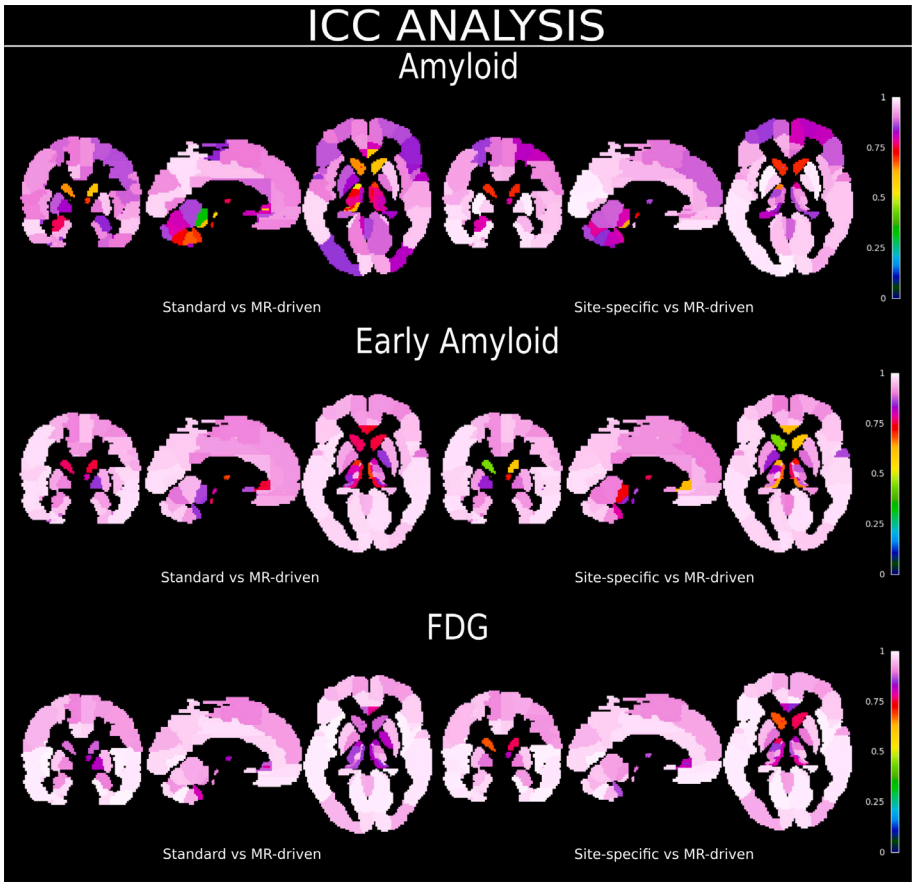

Fig. 3. Intraclass correlation coefficient (ICC) maps comparing the MR-driven, standard, and site-specific templates for three PET tracers: Amyloid, Early Amyloid, and FDG. The first column in each row shows the comparison between the standard and MR-driven templates, while the second column shows the comparison between site-specific and MR-driven templates. Higher ICC values (indicated by warmer colors) represent higher agreement, while lower values (cooler colors) represent more variability across the templates.

was chosen as the measure of central tendency due to its robustness against outliers.

All the statistical analyses were conducted using statsmodels [28], scipy [29] and PyReliMRI [30] Python libraries.

4. Results

The consistency of 166 ROIs was assessed using the ICC to evaluate the reliability of three template strategy generations. Specifically, the effectiveness of two approaches that do not use MRI (Site-specific and Standard templates) against the MR-driven approach, across three imaging modalities: amyloid, early amyloid and FDG was compared.

The ICC analysis results for each modality are presented in Fig. 3, providing a visual representation of the assessment for each ROI from the AAL3 Atlas. In particular, for:

- **Amyloid PET**
  - **Standard template vs MR-driven:** The median ICC was 0.822 (0.895–0.759), suggesting overall good agreement, though with notable variability in several regions. The ICC was highest in the Precuneus-L region (ICC = 0.975, ROI 71), indicating excellent agreement between the standard template and MR-driven methods. On the other hand, the lowest ICC value was observed in the Cerebellum-10-R region (ICC = 0.170, ROI 112), indicating poor agreement in this region.
  - **Site-specific vs MR-driven:** For the site-specific template, the median ICC value observed was 0.924(0.953–0.860), with the highest in the Calcarine-L region (ICC = 0.990, ROI 47), demonstrating excellent agreement. However, the Thal-Re-L region (ICC = 0.445, ROI 133) showed the lowest value.
- **Early Amyloid PET**
  - **Standard template vs MR-driven:** The median ICC value was 0.919 (0.955–0.847), suggesting good overall agreement across most regions. The highest ICC value was observed in the Temporal-Inf-R region (ICC = 0.980, ROI 94), however, the lowest ICC was found in the Thal-AV-R region (ICC = 0.493, ROI 122), reflecting moderate variability.
  - **Site-specific vs MR-driven:** The median ICC for this comparison was 0.927 (0.957–0.864), indicating good agreement between site-specific and MR-driven methods. Again the Temporal-Inf-R region had the highest ICC in the early amyloid modality (with the same value of ICC). Conversely, the Thal-LP-L region (ICC = 0.226, ROI 123) had the lowest ICC, showing significant variability.
- **FDG PET**
  - **Standard template vs MR-driven:** The median ICC value for the standard template comparison was 0.945 (0.972–0.8 99), reflecting generally strong agreement across regions. The highest ICC value was observed in the Insula-L region (ICC = 0.993, ROI 33), showing a high level of agreement. The lowest ICC was in the Thal-AV-R region (ICC = 0.641, ROI 122), indicating moderate agreement in this parcel.

– **Site-specific vs MR-driven:** The median ICC for this comparison was 0.948 (0.971–0.907), indicating strong agreement between site-specific and MR-driven methods. The Temporal-Inf-R region (ICC = 0.992, ROI 94) had the highest ICC value, while the lowest value was observed in the Thal-AV-L region (ICC = 0.407, ROI 121). For FDG, this analysis was performed also using the dementia-specific template proposed by Della Rosa et al. [17]. The results, shown in Figure 4 in the supplementary material, indicate a high agreement across all methods, particularly with the site-specific template.

5. Discussion

The present study investigated the differences between MR-driven and MR-free spatial normalization among three PET modalities.

This is especially critical given the increasing demand for diagnostic imaging for monitoring new treatments for Alzheimer's disease. In this context, this work is particularly relevant, as they recently validated a processing pipeline using only amyloid PET images to apply the Centiloid scale, explicitly to relieve the burden on conventional PET/CT systems [31].

To ensure a comprehensive comparison, three different templates were generated for each PET modality, one based on MR-driven normalization and two derived from MR-free approaches comparing them pairwise.

An excellent agreement with MR-free normalization for FDG modality in cortical regions was revealed, with ICCs exceeding 0.99 in areas such as the insula, inferior temporal lobe, and precuneus, and ICCs above 0.90 in other cortical regions. These results indicate that MR-free normalization is highly comparable to MR-driven in regions with elevated metabolic activity. These findings are consistent with the work of Li et al. [32], that achieved a strong correlations when comparing uptake values from manually defined ROIs (eight cortical regions and two subcortical regions) with r = 0.85–0.98.

Similarly, in this study an excellent agreement with MR-free normalization early amyloid template was founded, resulting in median ICC value of 0.927 (0.957–0.864). These findings further support the excellent performance of the MR-free spatial normalization approach using early-phase PET amyloid template, in line with previous report and extending to more regions [18].

Notably the current study provides novel evidence of similar reliability of spatial normalization behavior of early amyloid PET and FDG-PET templates. These findings reinforce the strong association between FDG-PET and early amyloid [7] including 18F-Flutemetamol images [33–35] and also support recent advancements in deep learning approaches for generating FDG-PET images from early-phase amyloid PET data, such as those proposed by Sanaat et al. [36].

Significant similarities between early amyloid and FDG modalities were observed in terms of regional agreement between MR-free and MR-driven normalization. Both modalities demonstrated strong consistency (ICC > 0.9) in regions such as the Precuneus, Frontal-Sup, and Temporal-Inf, suggesting that these areas remain stable and reliable for regional uptake estimation across different normalization approaches.

Slightly lower agreement was generally observed in comparisons using amyloid-derived templates with ICC median of 0.822 (0.895 - 0–759) in the comparison with the $^{15}O - H_2O$ template. This is consistent with the findings of Hsiao et al. [18], who reported that early-phase amyloid PET, which exhibits a perfusion-like pattern, provides more reliable and consistent spatial normalization compared to ligand-related late-phase templates. This is particularly crucial for amyloid radiotracers that show heterogeneous radioligand distribution in the cerebral cortex and the white matter depending on amyloid status. The results could suggest that early-phase amyloid PET is better suited for spatial normalization due to its lower inter-subject variability and improved anatomical correspondence. Nevertheless, perfusion dementia-related patterns might result in possible bias of the early amyloid template. The use, in this research, of a mixed population that includes various dementia subtypes, encompasses this potential limitation and improves the reliability of the late amyloid template by incorporating a greater degree of variance within a single group. As a consequence, the findings become more generalizable in a cohort typical for PET imaging, ensuring these conclusions hold across different pathological conditions and disease stages.

In this work, cerebellar and thalamic sub-regions, exhibited the greatest variability between different normalization approaches with (ICC <0.75). This might be related to the relatively small size of ROIs included in the AAL3 atlas with respect to PET spatial resolution. It enabled a more detailed regional analysis and therefore allowed to highlight the limitations of spatial normalization in smaller brain structures, where the task is more challenging. To investigate this, an additional analysis on whole cerebellum and whole thalamus structures was conducted, by aggregating all respective sub-regional ROIs. This resulted in increased agreement among all the normalization modalities with minimal ICC value of 0.920.

The proposed approach highlights the methodological robustness of the normalization strategies. By implementing a leave-one-out cross-validation scheme, the method ensures that each subject is excluded from the template building process, thereby preventing bias. The strong ICC values observed across a broad range of cortical and subcortical regions, including structures with inherently lower anatomical contrast such as the thalamus and cerebellum, underscore the reliability of the MR-free methods. Furthermore, the improved agreement achieved through the aggregation of smaller sub-regions suggests that the approach remains effective even in structurally complex or low-contrast areas.

A possible limitation of this study could be the use of a $^{15}O - H_2O$ template as the standard PET distribution reference for FDG spatial normalization procedures, which may not optimally represent the average distribution across these analyzed PET modalities [19]. To address this point, an additional spatial normalization analysis of FDG images was performed on FDG images using the FDG dementia-specific template proposed by Della Rosa et al. [17]. The results demonstrated a high agreement with the site-specific template generated in this study, with median ICC of 0.982(0.988–0.975), which was expected considering the similarity between the populations used to construct both templates. Interestingly, a strong agreement was also found in the comparison of Della Rosa FDG templates with $^{15}O - H_2O$ templates, with a median ICC of 0.969 (0.981–0.947). Moreover, for amyloid imaging, a key adjustment was introduced to mitigate the limitations of the $^{15}O - H_2O$ template. Specifically, a prior co-registration step was implemented between the early and standard phases of amyloid PET, using the CT image as an intermediary.

There are other intrinsic limitations that should be acknowledged. One lies in its moderate sample size, which was constrained by the strict inclusion criteria. Although this sample size may limit the generalizability of the findings, consistently high ICC values were observed across tracers and anatomical regions, indicating strong internal consistency. To further mitigate the effects of sample size limitations, a leave-one-out cross-validation procedure was employed during the site-specific template generation. This strategy enabled the assessment of each individual using a template derived from the remaining cohort, thereby simulating the inclusion of previously unseen cases and enhancing the methodological rigor of the analysis. Another limitation is the use of MR data acquired from two different 3T scanners. Although the acquisition protocol was harmonized, scanner-related variability might have introduced additional variance in MR-driven normalization, potentially affecting the generalizability of the results. However, it was not possible to specifically assess the effects of scanner variability, as the distribution of patients between the two scanners was highly unbalanced, preventing a statistically meaningful comparison. In this context, the work of Wagatsuma et al. [37] frames our limitations within the

broader challenge of PET harmonization. Their development of a novel phantom emphasizes the need for ground-truth references to assess processing accuracy and highlights the importance of tracer-specific tools for reliable quantification.

5.1. Conclusion

In conclusion, this study primarily focused on assessing, with spatial normalization approaches, the feasibility of MR-free versus MR-driven approaches. The results further demonstrated the strong agreement among these methods for FDG, early and late amyloid PET templates. Moreover, this study supports the preferential use of early amyloid template for spatial normalization of late amyloid images and highlight its similarity with FDG template.

Fundings

This work is partially supported by the Italian Ministry of Health through the grants GR-2018-12366779 and "Ricerca Corrente" projects, as well as by #NEXTGENERATIONEU (NGEU) and funded by the Italian Ministry of University and Research (MUR) under the National Recovery and Resilience Plan (NRRP), project MNESYS (PE0000006) – A Multiscale integrated approach to the study of the nervous system in health and disease (DN. 1553 11.10.2022) (CC, EN, MS).

Declaration of competing interest

The authors declare that they have no known competing financial interests or personal relationships that could have appeared to influence the work reported in this paper.

Appendix A. Supplementary data

Supplementary material related to this article can be found online at https://doi.org/10.1016/j.ejmp.2025.105182.

References

[1] Jack Jr. CR, Bernstein MA, Fox NC, Thompson P, Alexander G, Harvey D, Borowski B, Britson PJ, Whitwell JL, Ward C, Dale AM, Felmlee JP, Gunter JL, Hill DL, Killiany R, Schuff N, Fox-Bosetti S, Lin C, Studholme C, DeCarli CS, Krueger G, Ward HA, Metzger GJ, Scott KT, Mallozzi R, Blezek D, Levy J, Debbins JP, Fleisher AS, Albert M, Green R, Bartzokis G, Glover G, Mugler J, Weiner MW. The Alzheimer's disease neuroimaging initiative (ADNI): MRI methods. J Magn Reson Imaging 2008;27(4):685–91. http://dx.doi.org/10.1002/jmri.21049, URL https://onlinelibrary.wiley.com/doi/abs/10.1002/jmri.21049. _eprint: https://onlinelibrary.wiley.com/doi/pdf/10.1002/jmri.21049.

[2] McKhann GM, Knopman DS, Chertkow H, Hyman BT, Jack Jr. CR, Kawas CH, Klunk WE, Koroshetz WJ, Manly JJ, Mayeux R, et al. The diagnosis of dementia due to Alzheimer's disease: Recommendations from the National institute on Aging-Alzheimer's Association workgroups on diagnostic guidelines for alzheimer's disease. Alzheimer's Dement 2011;7(3):263–9.

[3] Frisoni GB, Fox NC, Jack Jr. CR, Scheltens P, Thompson PM. The clinical use of structural MRI in Alzheimer disease. Nat Rev Neurol 2010;6(2):67–77.

[4] Herholz K, Carter S, Jones M. Positron emission tomography imaging in dementia. Br J Radiol 2007;80(special_issue_2):S160–7.

[5] Fodero-Tavoletti MT, Cappai R, McLean CA, Pike KE, Adlard PA, Cowie T, Connor AR, Masters CL, Rowe CC, Villemagne VL. Amyloid imaging in Alzheimer's disease and other dementias. Brain Imaging Behav 2009;3:246–61.

[6] Curtis C, Gamez JE, Singh U, Sadowsky CH, Villena T, Sabbagh MN, Beach TG, Duara R, Fleisher AS, Frey KA, et al. Phase 3 trial of flutemetamol labeled with radioactive fluorine 18 imaging and neuritic plaque density. JAMA Neurol 2015;72(3):287–94.

[7] Valentina G, Silvia M, Marco P. Dual-phase amyloid PET: hitting two birds with one stone. Eur J Nucl Med Mol Imaging 2016;43:1300–3.

[8] Hammers A, Koepp MJ, Free SL, Brett M, Richardson MP, Labbé C, Cunningham VJ, Brooks DJ, Duncan J. Implementation and application of a brain template for multiple volumes of interest. Hum Brain Mapp 2002;15(3):165–74.

[9] Rusjan P, Mamo D, Ginovart N, Hussey D, Vitcu I, Yasuno F, Tetsuya S, Houle S, Kapur S. An automated method for the extraction of regional data from PET images. Psychiatry Res: Neuroimaging 2006;147(1):79–89.

[10] Rabinovici G, Furst A, O'neil J, Racine C, Mormino E, Baker S, Chetty S, Patel P, Pagliaro T, Klunk W, et al. 11C-PIB PET imaging in Alzheimer disease and frontotemporal lobar degeneration. Neurology 2007;68(15):1205–12.

[11] Morbelli S, Piccardo A, Villavecchia G, Dessi B, Brugnolo A, Piccini A, Caroli A, Frisoni G, Rodriguez G, Nobili F. Mapping brain morphological and functional conversion patterns in amnestic MCI: a voxel-based MRI and FDG-PET study. Eur J Nucl Med Mol Imaging 2010;37:36–45.

[12] Akamatsu G, Ikari Y, Ohnishi A, Nishida H, Aita K, Sasaki M, Yamamoto Y, Sasaki M, Senda M. Automated PET-only quantification of amyloid deposition with adaptive template and empirically pre-defined ROI. Phys Med Biol 2016;61(15):5768–80. http://dx.doi.org/10.1088/0031-9155/61/15/5768.

[13] Sun X, Liang S, Fu L, Zhang X, Feng T, Li P, Zhang T, Wang L, Yin X, Zhang W, et al. A human brain tau PET template in MNI space for the voxel-wise analysis of Alzheimer's disease. J Neurosci Methods 2019;328:108438.

[14] Zhang T, Nie B, Liu H, Shan B, Initiative ADN. Unified spatial normalization method of brain PET images using adaptive probabilistic brain atlas. Eur J Nucl Med Mol Imaging 2022;49(9):3073–85.

[15] Zhang T, Wu S, Zhang X, Dai Y, Wang A, Zhang H, Tian M. Spatial normalization and quantification approaches of PET imaging for neurological disorders. Eur J Nucl Med Mol Imaging 2022;49(11):3809–29. http://dx.doi.org/10.1007/s00259-022-05809-6.

[16] Ashburner J. SPM: a history. Neuroimage 2012;62(2):791–800.

[17] Della Rosa PA, Cerami C, Gallivanone F, Prestia A, Caroli A, Castiglioni I, Gilardi MC, Frisoni G, Friston K, Ashburner J, et al. A standardized [18 F]-FDG-PET template for spatial normalization in statistical parametric mapping of dementia. Neuroinformatics 2014;12:575–93.

[18] Hsiao I-T, Huang C-C, Hsieh C-J, Wey S-P, Kung M-P, Yen T-C, Lin K-J. Perfusion-like template and standardized normalization-based brain image analysis using 18F-florbetapir (AV-45/Amyvid) PET. Eur J Nucl Med Mol Imaging 2013;40(6):908–20. http://dx.doi.org/10.1007/s00259-013-2350-x.

[19] Gispert JD, Pascau J, Reig S, Martínez-Lázaro R, Molina V, García-Barreno P, Desco M. Influence of the normalization template on the outcome of statistical parametric mapping of PET scans. NeuroImage 2003;19(3):601–12. http://dx.doi.org/10.1016/S1053-8119(03)00072-7, URL https://www.sciencedirect.com/science/article/pii/S1053811903000727.

[20] Evans AC, Collins DL, Mills S, Brown ED, Kelly RL, Peters TM. 3D statistical neuroanatomical models from 305 MRI volumes. In: 1993 IEEE conference record nuclear science symposium and medical imaging conference. IEEE; 1993, p. 1813–7.

[21] Avants BB, Tustison N, Song G, et al. Advanced normalization tools (ANTS). Insight J 2009;2(365):1–35.

[22] Maes F, Vandermeulen D, Suetens P. Medical image registration using mutual information. Proc IEEE 2003;91(10):1699–722.

[23] Klein A, Andersson J, Ardekani BA, Ashburner J, Avants B, Chiang M-C, Christensen GE, Collins DL, Gee J, Hellier P, et al. Evaluation of 14 nonlinear deformation algorithms applied to human brain MRI registration. Neuroimage 2009;46(3):786–802.

[24] Liu S, Yang B, Wang Y, Tian J, Yin L, Zheng W. 2D/3D multimode medical image registration based on normalized cross-correlation. Appl Sci 2022;12(6):2828.

[25] Rolls ET, Huang C-C, Lin C-P, Feng J, Joliot M. Automated anatomical labelling atlas 3. Neuroimage 2020;206:116189.

[26] Liljequist D, Elfving B, Skavberg Roaldsen K. Intraclass correlation–A discussion and demonstration of basic features. PloS One 2019;14(7):e0219854.

[27] Koo TK, Li MY. A guideline of selecting and reporting intraclass correlation coefficients for reliability research. J Chiropr Med 2016;15(2):155–63.

[28] Seabold S, Perktold J. Statsmodels: Econometric and statistical modeling with python. In: 9th python in science conference. 2010.

[29] Virtanen P, Gommers R, Oliphant TE, Haberland M, Reddy T, Cournapeau D, Burovski E, Peterson P, Weckesser W, Bright J, van der Walt SJ, Brett M, Wilson J, Millman KJ, Mayorov N, Nelson ARJ, Jones E, Kern R, Larson E, Carey CJ, Polat İ, Feng Y, Moore EW, VanderPlas J, Laxalde D, Perktold J, Cimrman R, Henriksen I, Quintero EA, Harris CR, Archibald AM, Ribeiro AH, Pedregosa F, van Mulbregt P, SciPy 10 Contributors. SciPy 1.0: Fundamental algorithms for scientific computing in python. Nature Methods 2020;17:261–72. http://dx.doi.org/10.1038/s41592-019-0686-2.

[30] Demidenko M, Poldrack R. PyReliMRI: An open-source python tool for estimates of reliability in MRI data [Computer software]. 2023.

[31] Gandia-Ferrero MT, Torres-Espallardo I, Martínez-Sanchis B, Muñoz E, Morera-Ballester C, Sopena-Novales P, Álvarez-Sánchez L, Baquero-Toledo M, Martí-Bonmatí L. Amyloid brain-dedicated PET images can diagnose Alzheimer's pathology with centiloid scale. Phys Medica 2024;121:103345.

[32] Li Y, Rinne JO, Mosconi L, Pirraglia E, Rusinek H, DeSanti S, Kemppainen N, Någren K, Kim B-C, Tsui W, et al. Regional analysis of FDG and PIB-PET images in normal aging, mild cognitive impairment, and Alzheimer's disease. Eur J Nucl Med Mol Imaging 2008;35:2169–81.

[33] Boccalini C, Peretti DE, Ribaldi F, Scheffler M, Stampacchia S, Tomczyk S, Rodriguez C, Montandon M-L, Haller S, Giannakopoulos P, et al. Early-phase 18F-florbetapir and 18F-flutemetamol images as proxies of brain metabolism in a memory clinic setting. J Nucl Med 2023;64(2):266–73.

[34] Schmitt J, Palleis C, Sauerbeck J, Unterrainer M, Harris S, Prix C, Weidinger E, Katzdobler S, Wagemann O, Danek A, et al. Dual-phase β-amyloid PET captures neuronal injury and amyloidosis in corticobasal syndrome. Front Aging Neurosci 2021;13:661284.

[35] Seiffert AP, Gómez-Grande A, Villarejo-Galende A, González-Sánchez M, Bueno H, Gómez EJ, Sánchez-González P. High correlation of static first-minute-frame (FMF) PET imaging after 18f-labeled amyloid tracer injection with [18F] FDG PET imaging. Sensors 2021;21(15):5182.

[36] Sanaat A, Boccalini C, Mathoux G, Perani D, Frisoni GB, Haller S, Montandon M-L, Rodriguez C, Giannakopoulos P, Garibotto V, Zaidi H. A deep learning model for generating [18F]FDG PET Images from early-phase [18F]Florbetapir and [18F]Flutemetamol PET images. Eur J Nucl Med Mol Imaging 2024. http://dx.doi.org/10.1007/s00259-024-06755-1.

[37] Wagatsuma K, Miwa K, Yamao T, Kamitaka Y, Akamatsu G, Nakajima K, Miyaji N, Ishibashi K, Ishii K. Development of a novel phantom for tau PET imaging. Phys Medica 2024;123:103399.